Efficient Grid Treatment of the Time Dependent Schrödinger Equation for Laser-Driven Molecular Dynamics

Fang Li*, Xiangying Hao, Xiaogang Li

Laboratory of Optical Information Technology, School of Science, Wuhan Institute of Technology, Wuhan 430073, China.

Abstract. We present an efficient method to solve the time dependent Schrödinger equation for modeling the dynamics of diatomic molecules irradiated by intense ultrashort laser pulse without Born-Oppenheimer approximation. By introducing a variable prolate spheroidal coordinates and discrete variable representations of the Hamiltonian, we can accurately and efficiently simulate the motion of both electronic and molecular dynamics. The accuracy and convergence of this method are tested by simulating the molecular structure, photon ionization and high harmonic generation of H_2^+.

AMS subject classifications: 35Q41, 70H05, 70F07

Key words: Time-dependent Schrödinger equation (TDSE), Hydrogen molecule, non-Born-Oppenheimer approximation.

1 Introduction

The interaction of atoms and molecules with intense ultrashort laser pulses has attracted increasing attention. Particularly, the high-order harmonic generation (HHG) [1, 2], above threshold ionization (ATI) [3] and dissociation [4], are extensively investigated in recent years. By using the high-order harmonics, attosecond coherent x-ray source has been produced [5, 6]. Such attosecond pulses make a breakthrough to image the motion of an electron inside atoms, molecules [7, 8] and lots of new applications are also developed [9–13]. For all of these investigations, an accurate and efficient theoretical model is of great importance to faithfully describe the electronic and molecular dynamics and to understand the underlying physics.

---

*Corresponding author. *Email address:* lifang_wit@hotmail.com (F. Li)

The most accurate way to describe laser-atom and molecule interaction is *ab initio* solution of time-dependent Schrödinger equation (TDSE). This model has lead to remarkable advancements in understanding the strong field phenomena. Nevertheless, this approach is quite computationally demanding because of the long range Coulomb potential and the high nonlinearity in the strong laser field. To accurately represent the Coulomb singularity, dense grid points near the nuclear origin must be employed. On the other hand, Coulomb effect is a long interaction force and also both HHG and ATI rely on a rescattering process [14]. According to this model, the electron is first ionized, then oscillates in the laser field and finally rescatters with the parent nucleus. The amplitude of electron motion is E_0/ω_0^2 [14], where E_0 and ω_0 are the laser amplitude and wavelength, respectively. Therefore, to simulate the electron motion, the space region should be several times larger than E_0/ω_0^2. Typically, a wide region of several tens angstrom or even larger is needed. Consequently, even with the state-of-the-art computer, it is still a big challenge to directly solve the full-dimensional TDSE for laser-atom interaction involving more than two electrons [15]. Fortunately, single-active-electron (SAE) is proven to be a good approximation and has been successfully utilized for describing the HHG, ATI and other phenomena. Within the SAE approximation, direct numerical solution of TDSE for laser-atom interaction has been well established. Nevertheless, compared with atoms, the molecules have additional degree of freedom and more complicated structure, the physical phenomena of molecular HHG [16–20] and ATI [23–25] are richer. These processes have attracted more and more interests because of the applications of imaging of molecular orbital [26]. Due to the extra internuclear motion, the response of molecules to strong fields usually depends on the structure and alignment of the molecules [16, 27], thus making it more complicated than that of atoms [17, 28]. Currently, the simulation is generally concentrated on the simple diatomic molecule. Although several numerical methods have been proposed for solving the TDSE, previous theoretical studies are mostly restricted either to the Born-Oppenheimer approximation [21, 22, 29–32] or to reduced-dimensionality TDSE [16, 17, 33], which however seems questionable to give an accurate results in quantity [34]. Whilst the nuclear motion was shown to play an important role in molecular HHG [17], therefore, the non-Born-Oppenheimer approach is indeed necessary for most simply molecules. In this work, to achieve a faithful theoretical model, we present an efficient way to *ab initio* solve the three dimensional TDSE without Born-Oppenheimer approximation, including both the electronic and molecular dynamics of diatomic molecules irradiated by intense ultrashort laser pulse.

2   Theoretical model

In this work, we focus on the interaction of diatomic molecule with a linearly polarized laser field. The simplest diatomic molecular ion H_2^+ and its isotopes has been the basis of much study. Hence it is of special interest both in theory and experiment. Here we also set our model for treating H_2^+. The TDSE can be expressed as (atomic units (a.u.) are

used unless otherwise noted)

$$i\frac{\partial}{\partial t}\Psi(\mathbf{R},\mathbf{r},t)=[T_R(\mathbf{R})+T_e(\mathbf{r})+V_c(\mathbf{R},\mathbf{r})+V(t)]\Psi(\mathbf{R},\mathbf{r},t). \tag{2.1}$$

In this equation, T_R and T_e denote the kinetic energy operator for nuclear and electronic motions, respectively. V_c describes the Coulomb potential and $V(t)$ denotes the interaction of the external laser field. A full solution to this equation requires the propagation of a six-dimensional wave function. Unfortunately, this task is beyond our capability even using a supercomputer. We first consider the response of electron and nuclei in the external laser field. For molecular dynamics, the time scale of rotation is several hundreds femtosecond (fs) while the vibration is on the order of 10 fs. On the other hand, optical period of the driving laser field is 2.7 fs for the Ti:sapphire laser and electronic response is even faster. Therefore, the molecular rotation is much slower than the other processes and commonly can be neglected in the ultrashort laser field. We can only consider the nuclear motion along the polarization direction of the laser field. Moreover, since the molecule H_2^+ initially is on the ground state of $1s\sigma_g$, the azimuthal electron coordinate can be eliminated due to the symmetry in the linearly polarized field. Finally, we get a three-dimensional TDSE. Note that the azimuthal coordinate should be considered in a elliptically polarized field because of the broken of the cylindrical symmetry. Previous investigations usually solve the TDSE in the cylindrical coordinates [35–38] with the finite difference method. As mentioned above, the treatment of Coulomb potential requires very dense grid points near the nuclear origin and on the other hand, requires a wide region of the coordinate space. Even through scaled finite-difference method can be applied, a large number of grid points have to be adopted. An alternative way is solving the TDSE by discrete variable representations (DVR) [39], which is shown to be more efficient. Very accurate results can be obtained even with much less grid points [44] than the finite-difference method. However, in the cylindrical coordinate, the radial coordinate is suitable for the Lagrange DVR treatment. Finite difference method is still adopted in the axial coordinate [15] along which the laser is linearly polarized and a large number grid points are required. To overcome these problems, in this work, we solve the TDSE in the prolate spheroidal coordinates (ξ,η,ϕ), which is related to the Cartesian coordinates (x,y,z) by

$$x=\frac{R}{2}\sqrt{(\xi^2-1)(1-\eta^2)}\cos\phi, \tag{2.2}$$

$$y=\frac{R}{2}\sqrt{(\xi^2-1)(1-\eta^2)}\sin\phi, \tag{2.3}$$

$$z=\frac{R}{2}\xi\eta. \tag{2.4}$$

In these equations, R is the internuclear distance, $1\leq\xi<+\infty$, $-1\leq\eta\leq1$. Note that the prolate spheroidal coordinates were shown to be preferable compared with the other coordinates within the Born-Oppenheimer approximation [29,30]. However, for the non-

Born-Oppenheimer TDSE, we have to notice the movement of nuclei. Therefore we introduce a generalized prolate spheroidal coordinates, where the internuclear distance R can be changed from 0 to $+\infty$. We call this treatment variable prolate spheroidal (VPS) coordinates. We assume that H_2^+ is aligned on the axil z, along which the electric field is linearly polarized. Then the Coulomb potential between electron and two nuclei can be expressed by the following equations in VPS coordinates

$$V_c(\mathbf{R},\mathbf{r}) = -\frac{1}{|\mathbf{r}-R/2|} - \frac{1}{|\mathbf{r}+R/2|} + \frac{1}{R} = -\frac{4\xi}{R(\xi^2-\eta^2)} + \frac{1}{R}. \tag{2.5}$$

By using the length gauge, the interaction with the external field $E(t)$ is written as

$$V(t) = RE(t)\left(1+\frac{1}{1+2m_p}\right)\xi\eta, \tag{2.6}$$

where m_p is the mass of proton. The kinetic operator in VPS coordinates can be expressed as

$$T_R(\mathbf{R}) = -\frac{1}{2\mu_p}\frac{\partial^2}{\partial R^2}, \tag{2.7}$$

$$T_e(\mathbf{r}) = -\frac{1}{2\mu_e}\frac{4}{R^2(\xi^2-\eta^2)}\left[\frac{\partial}{\partial\xi}(\xi^2-1)\frac{\partial}{\partial\xi} + \frac{\partial}{\partial\eta}(1-\eta^2)\frac{\partial}{\partial\eta}\right], \tag{2.8}$$

where μ_p and μ_e are the reduced masses,

$$\mu_p = m_p/2 \tag{2.9}$$

and

$$\mu_e = \frac{2m_p}{2m_p+1}, \tag{2.10}$$

respectively.

The above treatment in VPS coordinates is suitable for adopting the DVR method. To efficiently solve the TDSE, one crucial issue is the discrete variable representation of the Hamiltonian. For clarity, we describe such a process in four subsections. In Subsection 2.1, we outline the basic idea of DVR method. In Subsection 2.2, we show the details of the treatment of electron coordinates, ξ and η. In Subsection 2.3, we discuss the discretization of the nuclear coordinates, R. Finally, the arithmetic of time propagation of the wavefunction is shown in Subsection 2.4.

2.1 DVR arithmetic

DVR is a method based on the orthogonal polynomials and Gaussian quadrature, which is shown to be an much efficient way in a number of applications. Here we present

the outline of DVR constructed from orthogonal polynomials, more details can be found in [39, 40].

For a complete set of orthogonal polynomials, $P_N(x)$, defined on a domain $a \leq x \leq b$ with the corresponding weight function $w(x)$, we have

$$\frac{1}{h}\int_a^b w(x)P_m(x)P_n(x) = \delta_{m,n}, \tag{2.11}$$

where h is a normalization constant. Then we can introduce a cardinal function $C_k(x)$ such that $C_k(x_j) = \delta_{kj}$, where

$$C_k(x) = \frac{1}{g_n(x_k)'}\frac{g_n(x)}{x-x_k}, \tag{2.12}$$

$$g_n(x) = \sqrt{w(x)/h}P_n(x). \tag{2.13}$$

$g_n'(x_k)$ denotes the first derivative of $g_n(x)$ at x_k and x_k $(k=1,2,\cdots,N)$ are the roots of $P_N(x)$. The basis function of DVR $f_i(x)$ is constructed from the cardinal function,

$$f_k(x) = \frac{1}{w_k}C_k(x), \tag{2.14}$$

which satisfies that $f_k(x_j) = \delta_{k,j}/\sqrt{w_k}$. By using the Gaussian quadrature,

$$\int_a^b dxF(x) \simeq \sum_{i=1}^N w_iF(x_j), \tag{2.15}$$

where w_j is the weight at x_j. According to the theory of Gaussian quadrature, this integration is exact as long as $F(x)$ is a polynomial with an order less than $2N-1$.

To show how to solve the TDSE with DVR method, we abbreviate the TDSE as

$$i\frac{\partial}{\partial t}\Psi(x,t) = [T+V(x,t)]\Psi(x,t). \tag{2.16}$$

Note that the meaning of the abbreviation x in Eq. (2.16) includes all the spatial coordinates. We expand the wavefunction in the basis $f(x)$,

$$\Psi(x,t) = \sum_i c_j(t)f_j(x), \tag{2.17}$$

where $c_j(t) = <f_j(x)|\Psi(x)>$. By substituting Eq. (2.17) into (2.16), TDSE can be written as

$$\sum_j \left[T_{kj}+V(x_j,t)\delta_{k,j}-i\frac{\partial}{\partial t}\delta_{k,j}\right]c_j(t) = 0, \tag{2.18}$$

where $T_{kj} = <f_k(x)|T|f_j(x)>$. In the following subsections, we will show the details of the solution of this set of equations.

2.2 Discretization of the electron coordinates

We first consider to apply the DVR method to the electron coordinates, ξ, η. For the coordinate η, we adopt the Legendre polynomial P_{N_y} and Legendre-Gauss quadrature [29]. According to the DVR algorithm shown above, the discrete grid points are the roots of Legendre polynomial and the weights are expressed by

$$\eta_j: \quad P_{N_y}(\eta_j) = 0, \tag{2.19}$$

$$w_j = \frac{1}{(1-\eta_j^2)(P'_{N_y}(\eta_j))^2}. \tag{2.20}$$

Note that N_y is the number of grid points used for η. The differentiation of a function $f(\eta)$ at η_j can be performed by

$$\frac{df(\eta_j)}{d\eta} = \sum_{j=1}^{N_y} D_{jj'} f(\eta_{j'}), \tag{2.21}$$

where $D_{jj'} = d_{jj'} P'_{N_y}(\eta_j)/P'_{N_y}(\eta_{j'})$ and $d_{jj'}$ is defined as $d_{jj'} = \frac{1}{\eta_j - \eta_{j'}}$ if $j \neq j'$ and $d_{jj} = \frac{\eta_j}{1-\eta_j^2}$. It should be noted that $f(\eta)$ has to be a continuous function. Otherwise the above equation will fail. For the interaction of molecules and laser pulse, the time dependent wave function always satisfies this requirement.

On the other hand, we consider the radial coordinate ξ. Note that the maximum of ξ can not be infinite in practical simulations. We generally adopt a value L that is large enough for electron's motion. For convenience, we first map the coordinate ξ to the range $[-1,1]$

$$\xi = 1 + \alpha \frac{1+x}{1-x+\frac{2\alpha}{L-1}}, \tag{2.22}$$

where α is a mapping parameter. The advantage is that the density of the grid points can be adjusted by changing the parameter α [29]. Usually, more grid points are selected near the origin to faithfully describe the Coulomb potential. The variable x is selected as the roots of the difference of two Legendre polynomials, i.e.,

$$x_k: \quad P_{N_x}(x_k) - P_{N_x+1}(x_k) = 0. \tag{2.23}$$

Note that $N_x + 1$ roots can be obtained from this equation, however the root $x_k = 1$ is selected as the boundary as [29]. We adopt the Legendre-Gauss-Radau quadrature, the corresponding weights are

$$w_k = \frac{1}{(N_x+1)^2} \frac{1+x_k}{P_{N_x}(x_k)^2}. \tag{2.24}$$

The differentiation of a function $f(x)$ can be calculated by

$$\frac{df(x_k)}{dx} = \sum_{k=1}^{N_x+1} D_{kk'} f(x_{k'}), \tag{2.25}$$

where

$$D_{kk'} = d_{kk'} \frac{(1+x_{k'})P_{N_x}(x_k)}{(1+x_k)P_{N_x}(x_{k'})}, \qquad (2.26)$$

and $d_{N_x+1,N_x+1} = N_x(N_x+2)/4$, $d_{kk'} = \frac{1}{x_k-x_{k'}}$ if $k \neq k'$ and $d_{kk} = -\frac{1}{2(1+x_k)}$. By substituting these formulas to Eq. (2.8), we can get the discrete form of the kinetic operator. Note however that the Hamiltonian is a full matrix with this DVR arithmetic. Recently, the DVR method has been combined with the finite element method, called FEDVR [41], which provides an even more flexible approach to adopt the size of the elements and the number of points in each element. Moreover, FEDVR leads to a sparse representation of the Hamiltonian matrix. This feature enables us to save the computational memory and may also to efficiently parallelize the computation [42, 43].

2.3 Discretization of the nuclear coordinates

The nuclear coordinate R can be treated with the same way as that to the electron coordinates. However, consider the oscillation motion of the molecular wavepacket, we prefer to adopt the sine polynomial as the basis function. The grid points are uniformly selected in the range $[R_{\min}, R_{\max}]$, i.e., $r_l = R_{\min} + \Delta(l-1)$, where $l = 1, 2, \cdots, N$ and $\Delta = (R_{\max} - R_{\min})/(N-1)$. The kinetic operator T_R can be simply calculated as $-\frac{1}{2\mu_p}D_{ll'}$, where

$$D_{ll'} = (-1)^{(l-l'-1)} \frac{1}{(l-l')^2}, \quad l \neq l', \qquad D_{ll} = -\pi^2/6. \qquad (2.27)$$

2.4 Arnoldi time propagator

In this section, we discuss the propagation of wavepacket in the time domain. The TDSE can be abbreviated as

$$i\frac{\partial}{\partial t}\Psi(x,t) = H\Psi(x,t). \qquad (2.28)$$

Note that the wave function and Hamiltonian become a vector and matrix after the discretization of the spatial coordinates. The time propagation can be expressed by $\Psi(t + \delta t) = \exp[-iH(t)\delta t]\Psi(t)$. Several algorithms have been proposed to solve this exponentials evolution, such as the split operator [45], Runge-Kutta [30] and Taylor series [15] methods. The split operator and Runge-Kutta methods usually achieve an accuracy of $(\delta t)^2$ and $(\delta t)^4$, respectively. The Taylor series method expresses the exponentials propagation operator by polynomials series, which can provide a higher order accuracy but is not efficient. In this work, we adopt the Arnoldi algorithm, which can offer an accurate and efficient treatment of the matrix exponentials [15, 40]. To apply the Arnoldi algorithm, we construct the Krylov subspace spanned by Ψ, $H\Psi, \cdots, H^m\Psi$ with $0 \leq m \leq M$. Orthonormalizing the basis vectors by the Gram-Schmidt procedure produces a new orthogonal set of vectors, which can be written as $q_0, q_1, \cdots, q_M$. Let Q denotes the matrix

formed by the M+1 vectors $[q_0, q_1, \cdots, q_M]$, we define a new matrix S, which is iteratively calculated by

$$S_{j,k-1} = q_j^\dagger q_k, \qquad q_k = q_k - S_{j,k-1} q_j, \qquad j = 1, 2, \cdots, k-1, \qquad (2.29)$$

$$S_{k,k-1} = \sqrt{|q_k|}, \qquad q_k = q_k / S_{k,k-1}, \qquad k = 2, 3, \cdots, M. \qquad (2.30)$$

S is the Krylov subspace Hamiltonian, we have $S = Q^\dagger H Q$. The exponential time propagation can be performed by

$$\exp[-iH(t)\delta t] \simeq Q \exp(-iS\delta t) Q^\dagger. \qquad (2.31)$$

S is typically a traditional matrix with a dimension of $(M+1)^2$. In practical simulation, M usually is set to about 20, therefore, $\exp(-iS\delta t)$ can be easily exponentiated by diagonalizing S. Note that Arnoldi algorithm is correct to the order of δt^{M+1} in time. Therefore the accuracy can be improved by increasing M or by reducing δt. Moreover, we should note that the Arnoldi method in principle is not unitary. The truncation error can be approximately estimated by $H^{(M+1)} \Psi \delta t^{(M+1)}$. We can expand the wave function as $\Psi = \sum_{E_n \leq 0} C_n \psi_n + \sum_{E_n > 0} C_n \psi_n$ where ψ_n is the eigenfunction and E_n is the corresponding eigenenergy. Hence the first term corresponds to the bound states and the second term corresponds to the continue states.

$$H^{(M+1)} \sum_{E_n \leq 0} C_n \psi_n \delta t^{(M+1)} = \sum_{E_n \leq 0} C_n E_n^{(M+1)} \psi_n \delta t^{(M+1)} < \sum_{E_n \leq 0} C_n |E_0|^{M+1} \delta t^{(M+1)}, \qquad (2.32)$$

where E_0 is the eigenenergy of the ground state, i.e., the ionization energy. As mentioned above, the maximum energy of the electron obtained in the laser field is $3.17U_p$. Then we can show that

$$H^{(M+1)} \sum_{E_n > 0} C_n \psi_n \delta t^{(M+1)} < \sum_{E_n > 0} C_n |3.17U_p|^{M+1} \delta t^{(M+1)}. \qquad (2.33)$$

For an intensity of 3×10^{14} W/cm^2, $3.17U_p$ is 1.97 a.u. for the Ti:saphire laser (800 nm). The ionization energy of H$_2^+$ is about 1.1 a.u. Hence the truncation error is estimated to be less than $(1.97\delta t)^{M+1}$. Generally, δt is about 0.05 a.u., the truncation error is less than 10^{-21} when $M = 20$. It is small enough for the double-precision values adopted in the simulation. In this situation, the Arnoldi method can be considered as unitary.

Before we proceed to the simulation, we briefly estimate the required resource for the calculation. For the single-electron system discussed above, the number of the grid points related to the wavefunction is $N_\xi N_\eta N_R$ and the Hamiltonian is a matrix of $(N_\xi N_\eta N_R)^2$, which typically requires a memory of about several Gigabyte. However, the required memory grows exponentially with increasing the number of the degrees of freedom. For the two-electron system, e.g., H$_2$ molecules, we also need to consider the azimuthal angle because of the Coulomb interaction between the electrons. In this case, the number of

the grid points related to the wavefunction is $(N_\xi N_\eta)^2 N_a N_R$ and the size of Hamiltonian is $(N_\xi N_\eta)^4 N_a^2 N_R^2$, where N_a denotes the number of grid points related to the azimuthal angle. Of course, we do not need to save the full Hamiltonian matrix in the memory (it is actually very difficult for such a huge matrix). However, we have to calculate the multiplication of the Hamiltonian and wavefunction, which is very time consuming and parallel calculation is required. For larger systems including more than 2 electrons, it becomes very difficult for *ab initio* solving the full dimensional TDSE. Alternative model, such as time dependent Hartree-Fock or density function theory, can be considered. In this case, the DVR and Arnoldi time propagator methods shown above still work efficiently.

3   Simulation results and discussions

To illustrate the algorithm outlined above, we simulate the electronic dynamics of H_2^+ in the presence of a time-dependent intense laser field. In our simulation, we have adopted 60 and 15 Legendre basis functions for treating the electron coordinates of ξ, η, respectively. The mapping parameter $\alpha = 160$ and $L = 40$ a.u.. While 80 sine polynomials are used to discretize the nuclear coordinate R and the step $\Delta R = 0.25$ a.u. Note that for the nuclear coordinates, discrete grid points are evenly spaced. However, as mentioned above, the discrete grid points are not uniformly located for the electron coordinates. Fig. 1 shows the distribution of the discrete grid points in the two dimensional (x and z) electron coordinates, where the internuclear distance R is assumed to be 2 a.u. We can see from Fig. 1 that dense grid points are located near the cores of the nuclei, therefore the Coulomb potential can be described more accurately. On the other hand, apart from the nuclei, the Coulomb potential becomes very weak and smooth and therefore sparse grid points are adopted. Note that the representation of the Coulomb potential is very
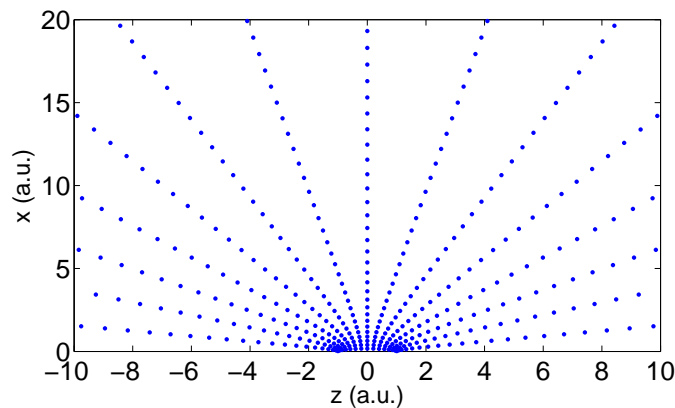

Figure 1: (Color online) Distribution of the discrete grid points in the two-dimensional electron coordinates.

computationally demanding because of the singularity and the long range interaction. The commonly-used finite different method adopts uniform grid points. A large number of grid points are required for an accurate representation of the Coulomb potential. By contrast, DVR method adopts nonuniformly spaced grid points, which enables us to overcome this problem by adjusting the density of the grid points. Such a method is much more efficient.

Because DVR method enables us to efficiently describe the Coulomb potential, we can simulate the electronic structure of the molecule H_2^+ very accurately. Table 1 shows the eigenenergies for the first 12 electric bound states. For comparison, eigenvalues reported in [46] are also presented. We can see that for the ground and first two bound states, more than 13 digit accuracy can be achieved. About 10 digit accuracy can be achieved for the states from 3P to 4D. The eigenstate becomes more and more dense as increasing the eigenenergy, nevertheless high accuracy still can be achieved. Note that the number of the grid points and basis functions we adopted is intended to accurately solve the TDSE involving the continuum states. Actually, much less basis functions (about 15) is sufficient to achieve a 14 digit accuracy for the ground state.

Table 1: Eigenenergies of the bound states of H_2^+ obtained with our method and [46]. The internuclear distance is assumed to be 2 a.u.

State	Energy in present work	Energy in Ref. [46]
1S SIGMA G	-0.602634214494947	-0.6026342144949
2P SIGMA U	-0.167534392202413	-0.1675343922024
2P PI U	0.0712281801041407	0.07122818010413
2S SIGMA G	0.139135124660516	0.1391351246617
3P SIGMA U	0.244586834913515	0.2445868349143
3D SIGMA G	0.264222371174451	0.2642223711745
3D PI G	0.273300373356347	0.2733003733563
3S SIGMA G	0.322318954873545	0.3223189549591
4P SIGMA U	0.362687075637494	0.3626870757439
4D SIGMA G	0.369208122266617	0.3692081223681
4F SIGMA U	0.373289868596324	0.3733561298504
5F SIGMA U	0.419155465395248	0.4191557039293
5F SIGMA G	0.419626476198921	0.4196265315607

Lots of the molecular dynamics, such as dissociation, bond soft, can be understood from the potential curve of eigenenergy as a function of internuclear distance [usually called Born-Oppenheimer (BO) potential]. Therefore, the accuracy simulation of the BO potential is of great importance for representing the molecular dynamics. Fig. 2 shows the BO potential of the $1s\sigma_g$ and $2p\sigma_u$ states of H_2^+ obtained with our numerical method. We can see that the results agree quite well with the data in [46].

For another application of our model, we have considered the ionization process of H_2^+ subjected to an intense ultrashort laser pulse. The electric field is taken as linearly
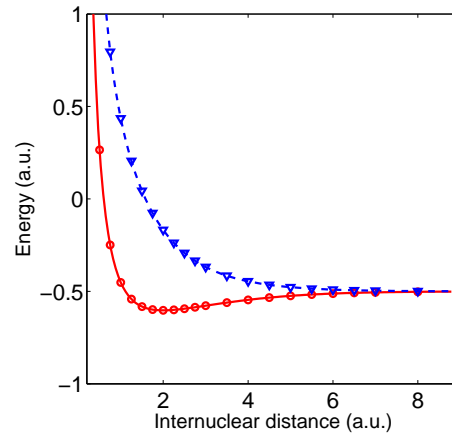
Figure 2: (Color online) BO potential curve of the $1s\sigma_g$ and $2p\sigma_u$ states of H_2^+. Solid and dashed lines are obtained with our method and the dots and triangles are the data in [46]. The solid line and dots correspond to the $1s\sigma_g$ state. The dashed line and triangles correspond to the $2p\sigma_u$ state.

polarized, which can be expressed by [47]

$$E(t) = E_0 \sin\left(\frac{\pi t}{T}\right)^2 \sin(\omega t + \phi_0). \tag{3.1}$$

E_0 is the laser amplitude, ω and ϕ_0 are the frequency and carrier-envelope phase [48], respectively. The time is in the range from 0 to T where $T = nT_0$ and T_0 is the optical cycle of the driving laser pulse. We adopt a few-cycle laser pulse, $T = 4T_0$, and a wavelength of 800 nm. The carrier-envelope phase is set to be 0. The laser intensity is 3×10^{14} W/cm^2. Fig. 3(a) shows the temporal profile of the electric field. TDSE is solved with the method outlined above. The initial state is taken as the ground state $1s\sigma_g$. Arnoldi method with a 30 order accuracy is used to simulate the time propagation of the wavefunction. The time step is 0.05 a.u. In the time propagation process, wave packets that reach the boundary can be reflected, causing artifact effects of ionization. To eliminate these reflections, we have adopted an absorbing boundary which smoothly absorbs the wave function reflected from the boundary.

Fig. 3(b) shows the population of nonionized electron of H_2^+ subjected in the few-cycle laser pulse. We can see that the population drops step by step, which corresponds the ionization at the most intense peaks, P_1, P_2 and P_3 of the driving field. To confirm the convergence of our algorithm, we have performed a simulation by using the Arnoldi method with a 40 order accuracy. The good agreement between these two simulations demonstrates the convergence of our algorithm. We have also performed a lots of test simulations, usually 30 and higher order Arnoldi propagator enable us to get a good accuracy. Of course, a lower order Arnoldi propagator can be adopted when reducing time step δt. However, because the accuracy of Arnoldi propagator is proportional to $(\delta t)^n$. The computing efforts of reducing δt by half are similar to that of increasing n by
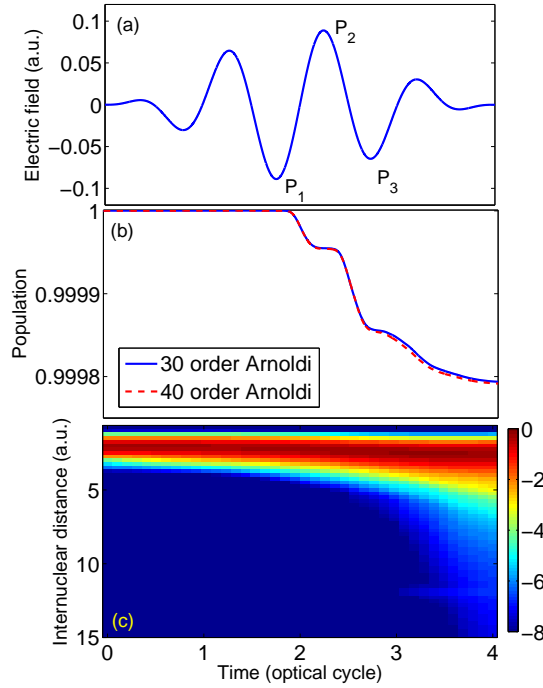
Figure 3: (Color online) (a) The electric field with an intensity of 3×10^{14} W/cm^2 and pulse duration of 4 optical cycles. The central wavelength is 800 nm. (b) The population of the nonionized electrons of H$_2^+$ subjected in the laser field. The solid line and dashed line correspond to the simulation by using the 30 and 40 order Arnoldi methods, respectively. (c) The evolution of the molecular wave packet in the laser field shown in (a). Note that logarithmic scale is used for the color bar.

a factor of 2. Since δt is a small value, $(\delta t)^n$ decreases very fast as increasing n. In other words, it is more efficient to improve the accuracy by increasing n.

The non-Born-Oppenheimer model shown in above enables us to investigate not only the electric motion, but also to investigate the molecular dynamics. Fig. 3(c) shows the evolution of the molecular wave packet driven by the few-cycle laser pulse. The probability distribution of molecular wave packet is calculated by integrating the electron motion, i.e., $P(R,t)=(R/2)^3\int d\xi\int d\eta(\xi^2-\eta^2)\Psi(R,\xi,\eta,t)^*\Psi(R,\xi,\eta,t)$. Note that the term $\xi^2-\eta^2$ can be eliminated by introducing $\psi=\Psi/\sqrt{\xi^2-\eta^2}$. We can see that H_2^+ initially is on the equilibrium state with an internuclear distance of 2 a.u. In the leading edge of the few-cycle pulse, the molecule expands very slowly. However, as the laser intensity increases, the molecular wave packet rapidly expands and the internuclear distance increases to 6 a.u. at the trail of the driving pulse.

Moreover, we have investigated the high harmonics generation with the above model. The high harmonic spectrum is calculated via the Fourier transform of the dipole momentum, which can be defined either in the length or acceleration forms by $d_L(t)=<\Psi|z|\Psi>$,
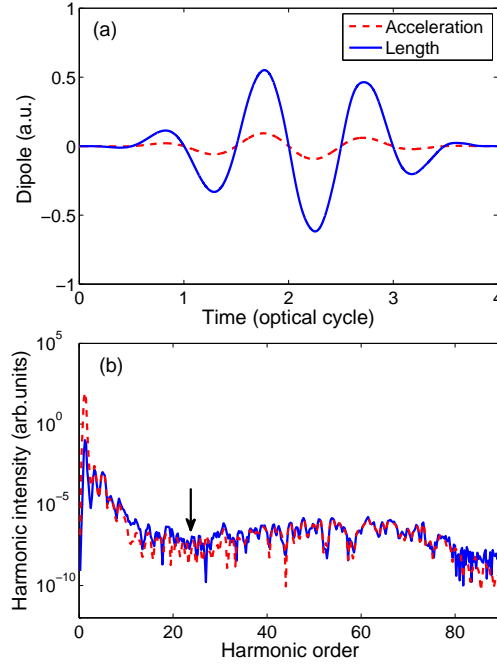
Figure 4: (Color online) (a) The dipole momentum in the length and acceleration forms. Other parameters are same with Fig. 3. (b) The harmonic spectra calculated from the length (blue solid line) and acceleration (red dashed line) forms of the dipole momentum, respectively.

$d_a(t) = <\Psi | \partial_t^2 z | \Psi>$, respectively. The harmonic spectrum are calculated accordingly,

$$P_L = \frac{\omega^4}{4\pi c^3} | d_L(\omega)|^2, \tag{3.2}$$

$$P_a = \frac{1}{4\pi c^3} | d_a(\omega)|^2, \tag{3.3}$$

where $d_L(\omega)$ and $d_a(\omega)$ denote the Fourier transform of d_L an d_a. Note that $d_L(\omega)\omega^4 = d_a(\omega)$ and these two approaches become equal when the simulation is converged. Therefore, it is generally used to check the convergence of the numerical simulation. Fig. 4(a) shows the dipole momentums in the length and acceleration forms, respectively. The corresponding harmonic spectra are shown in Fig. 4(b). The good agreement between these two spectra demonstrates the convergence of our simulation. On the other hand, it is worthy noting that the harmonic spectra clearly show a "dip" around the 23rd harmonic. This can be attributed to the destruct interference of the molecular wavepacket [30, 49]. A similar "dip" structure has been demonstrated with the Born-Oppenheimer approximation model [30, 49]. However, it has not been demonstrated with the non-Born-Oppenheimer model. Compared with [49], we can see that the "dip" becomes shallower in our model. It is possibly due to the influence of the nuclear motion (see Fig. 3(c)).
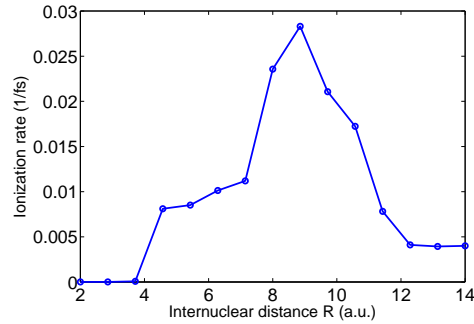
Figure 5: (Color online) The ionization rate as a function of internuclear distance. The laser pulse duration is 25 optical cycle (see Fig. 6(a)). The laser intensity is 1×10^{14} W/cm^2 and central wavelength is 1064 nm.

The above simulation adopts a few-cycle pulse, to further test our model, we have investigated the electronic and molecular dynamics in a long driving laser pulse. One interesting phenomena of molecules is that the ionization becomes unexpected high at some critical internuclear distance, which is called charge resonance enhanced ionization (CREI) [50]. This process plays an important role for lots of ultrafast process in the interaction of molecules and intense lasers. Lots of efforts have been paid to the simulation of CREI by different groups [22, 50, 51]. All these works adopted the model of solving the TDSE in cylindrical coordinates (ρ, z, R). As mentioned in Section 2, Lagrange DVR method can be applied to discretize the radical coordinate ρ. Then denser grid points can be adopted near the origin. However, the axial coordinates z varies from $-\infty$ to ∞, either Lagrange or Legendre DVR methods are not suitable. Of course, the DVR methods based on the sinc and fourier functions can be applied. However, these DVR methods adopt uniformly distributed grid points. It does not show significant advantages compared with the Finite definite and fast Fourier transform methods. On the other hand, since the laser field is polarized along the axial direction, a larger number of grid points usually have to be used in the simulation. By contrast, our model based on the VPS is more efficient. For comparison, we have simulated the CREI process in a long driving pulse. As [22, 50, 51], the central wavelength is 1064 nm and the peak intensity of the laser pulse is 1×10^{14} W/cm^2. The total pulse duration $T = 25T_0$. The laser field is switched on in the first 5 optical cycles then kept on a constant intensity for 15 cycles and is switched off in the last 5 cycles [see Fig. 6(a)]. In our simulation, we have adopted 72 and 24 Legendre basis functions for discretizing the coordinates of ξ, η, the mapping parameter $\alpha = 160$, $L = 40$ a.u. and the internuclear distance varies from 1 a.u. to 15 a.u. The ionization rate is calculated with the same procedure as [50,51]. We first assume that the internuclear distance is fixed (e.g., R=6 a.u. as shown in Fig. 6) and then calculate the time dependent wavefunction. From the norm of the wavefunction, we can calculate the population of the nonionized electrons as a function of time, which is denoted as $N(t)$. As [50,51], $N(t) = \exp(-\Gamma t)$ where Γ is the ionization rate. It can be obtained by $\Gamma(t) = -dln[N(t)]/dt$. Note that the laser amplitude is constant from t=5 T$_0$ to 20 T$_0$.

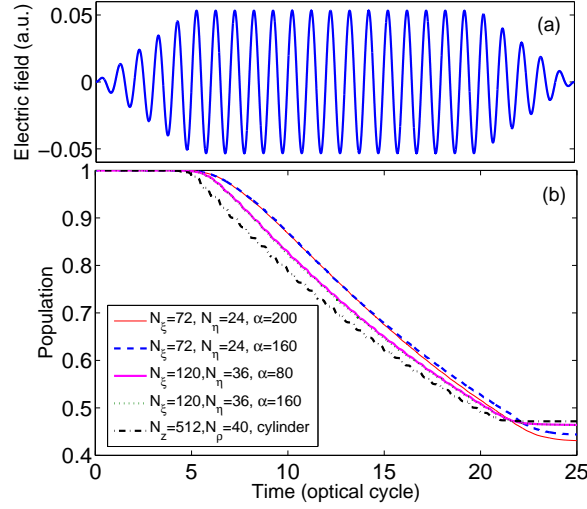Figure 6: (Color online) (a) The electric field with a duration of 25 optical cycles. The laser intensity is 1×10^{14} W/cm^2 and central wavelength is 1064 nm. (b) The population of the nonionized electrons as a function of time. The internuclear distance is set to be 6 a.u. and different grids were adopted for discretizing the coordinates of ξ, η.

Therefore the overall ionization rate can be calculated by averaging $\Gamma(t)$ from 5 T$_0$ to 20 T$_0$ [50, 51]. Fig. 5 shows the ionization rate as a function of internuclear distance. We can see two maximums, the first one is around 4-6 a.u. and the other one appears around 8-10 a.u.. The ionization rate is highest (=0.28 1/fs) at 9 a.u. Such results agree very well the previous simulations [22, 50, 51].

Furthermore, we have changed the number of grid points in our simulation. In Fig. 6(b), the population of the nonionized electron is presented as a function of time. Different grid points and mapping parameters were adopted for discretizing the coordinates of ξ, η. As shown in this figure, the ionization is fully converged when $N_\xi = 120$ and $N_\eta = 36$ in our method. The change of mapping parameter α does not influence the results either. Even through the ionization is very high at the end of laser pulse ($\simeq 65\%$), the deviation is less than 2% when the number of grid points N$_\xi$ and N$_\eta$ are reduced to 72 and 24. We have also changed the spatial region L to 60 and 80 a.u. and converged results are obtained. For comparison, we have also simulated this process by solving the TDSE in cylindrical coordinate. As [22], Lagrange DVR method is applied in the radical coordinate ρ and N$_\rho = 40$. Uniformly distributed grid points are adopted in the axial direction and 512 points were used. The result agrees very well with our simulation. However, the required grid points are approximately 5 times higher in the cylindrical coordinates. Accordingly, the required memories for the wavefunction and Hamiltonian are 5 and 25 times larger than our model. Note the evolution of the population is slightly different for these simulations. It is because the wavefunction is integrated with different grids as
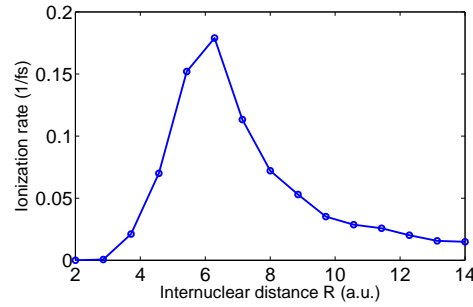
Figure 7: (Color online) The ionization rate as a function of internuclear distance. The laser intensity is 3×10^{14} W/cm^2 and the central wavelength is 800 nm. Other parameters are the same with Fig. 5.

changing the number of grid points. This artifact does not influence the final result, so the results are convergent at the end of the laser pulse.

On the other hand, we have calculated the CREI at slightly higher laser intensity of 3×10^{14} W/cm^2 with our model. Note that Williams *et al.* [52] have experimentally estimated the internuclear dependence of the ionization rate in an intense laser field. However, only one maximum was found by Williams *et al.* and the highest ionization appears at 6 a.u.. In Fig. 7, the ionization rate is presented as a function of internuclear distance. Different from Fig. 5, the ionization indicates only one maximum at 6 a.u., which is in agreement with the experiment [52].

With the development of the laser technology, it becomes possible to produce an intense laser pulse in the infrared region. In recent years, there is an increasing interest to investigate the ultrafast dynamics using a infrared laser pulse in recent years [53, 54]. However, the CREI in the infrared region has not been simulated to the best of our knowledge. In Fig. 8, we show the ionization rate as a function of internuclear distance in a
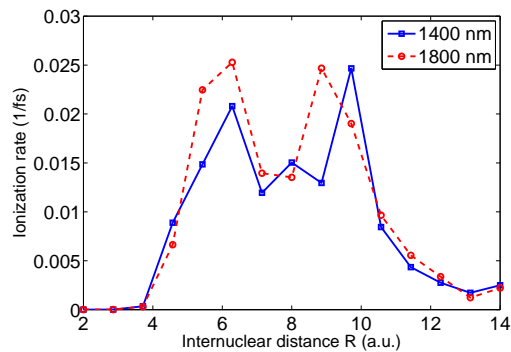

Figure 8: (Color online) The ionization rate as a function of internuclear distance. The central wavelengths are 1400 nm (solid line) and 1800 nm (dashed line), respectively. $N_{\xi}=200$, $N_{\eta}=24$, $L=120$, $\alpha=480$ and other parameters are the same with Fig. 5.

1400-nm and 1800-nm laser fields, respectively. The laser intensity is same with Fig. 5, i.e., 1×10^{14} W/cm^2. Note that the oscillation amplitude of the electron motion becomes larger in the infrared field. Therefore, a spatial range of 120 a.u. and larger number of grid points ($N_\xi = 200$, $N_\eta = 24$) were adopted in this simulation. From Fig. 8, we can see that two maximums are presented at 6 and 10 a.u., respectively. However, the ionization becomes higher around 6 a.u. compared with Fig. 5.

4 Conclusions

An efficient method to *ab initio* solve the time dependent Schrödinger equation without Born-Oppenheimer approximation is presented. Our treatment is based on the variable prolate spheroidal coordinates and discrete variable representations of the Hamiltonian. This non-Born-Oppenheimer model has enabled us to visualize both the electronic and molecular dynamics. With this model, we have accurately simulated the electronic structure and dynamics of H_2^+ subjected to an intense ultrashort laser pulse. Moreover, the evolutions of molecular wave packet and high harmonic generation are accurately simulated and the "dip" structure of the harmonic spectrum is demonstrated without the Born-Oppenheimer approximation. Also the CREI of H_2^+ subjected to an infrared (1400 and 1800 nm) driving pulse is simulated. Note that even through the simulation is shown for hydrogen molecular ion, the method presented in this work gives a general approach for modeling the diatomic molecular dynamics subjected to the intense laser fields. It can be generated to a wide variety of applications.

Acknowledgements

References

[1] A. Mcpherson, et al., J. Opt. Soc. B, 4 (1987), 595.
[2] M. Ferray, et al., J. Phys. B, 21 (1988), L31.
[3] P. Agostini and F. Fabre, and G. Mainfray, and G. Petite, and N. Rahman, Phys. Rev. Lett., 42 (1979), 1127.
[4] A. Giusti-Suzor and F. H. Mies , Phys. Rev. Lett., 68 1992, (3869).
[5] M. Hentschel, et al., Nature (London), 414 2001, 509.
[6] P. M. Paul, et al., Science, 292 (2001), 1689.
[7] M. Uiberacker, et al., Nature (London), 466 (2007), 627.
[8] M. Swoboda, et al.,, Phys. Rev. Lett., 104 (2010), 103003.
[9] A. D. Bandrauk and S. Chelkowski, and H. S. Nguyen, Int. J. Quantum Chem., 100 (2004), 834.
[10] P. F. Lan, et al., Phys. Rev. A, 76 (2007), 043808.

[11] P. F. Lan and P. X. Lu, Phys. Rev. A , 77 (2008), 013405.
[12] S. X. Hu, Phys. Rev. A , 83, (2011), 041401(R).
[13] W. Y. Hong and P. X. Lu, and P. F. Lan, and Q. B. Zhang, and X. B. Wang, Opt. Express , 17 (2009), 5139.
[14] P. Corkum, Phys. Rev. Lett., 71 (1993), 1994.
[15] D. Dundas and K. J. Meharg, and J. F. McCann, and K. T. Taylor, Eur. Phys. J. D, 26 (2003), 51.
[16] M. Lein, Phys. Rev. Lett., 94 2005, 053004.
[17] A. D. Bandrauk and S. Chelkowski, and S. Kawai, and H. Lu, Phys. Rev. Lett., 101 2008, 153901.
[18] P. F. Lan and et al., Opt. Express, 16 (2008), 17542.
[19] Q. B. Zhang and P. X. Lu, and W. Y. Hong, and Q. Liao, and S. Y. Wang, Phys. Rev. A, 80 (2009), 033405.
[20] M. Y. Qin and X. S. Zhu, and Q. B. Zhang, and W. Y. Hong, and P. X. Lu, Opt. Express, 19 (2011), 25084.
[21] P. F. Lan and P. X. Lu, and W. Cao, and X. L. Wang, and W. Y. Hong, Opt. Lett., 32 (2007), 1186.
[22] L. Y. Peng and J. F. McCann, and D. Dundas, and K. T. Taylor, and I. D. Williams, J. Chem. Phys., 120 (2004), 10046.
[23] M. Lein and J. P. Marangos, and P. L. Knight, Phys. Rev. A, 66 (2002), 051404(R).
[24] T. Zuo and A. D. Bandrauk, and P. B. Corkum, Chem. Phys. Lett., 259 (1996), 313.
[25] X. S. Zhu and Q. B. Zhang, and W. Y. Hong, and P. X. Lu, and Z. Z. Xu, Opt. Express, 19 (2011), 13722.
[26] J. Itatani et al., Nature (London), 432 (2004), 867.
[27] C. Chuang, et al. Opt. Express, 19 (2011), 5627.
[28] X. S. Zhu, et al., Opt. Express, 19 (2011), 436.
[29] D. A. Telnov and Sh. I. Chu, Phys. Rev. A, 76 (2007), 043412.
[30] G. L. Kamta and A. D. Bandrauk, Phys. Rev. A, 70 (2004), 011404(R).
[31] T. K. Kjeldsen and L. A. A. Nikolopoulos, and L. B. Madsen, Phys. Rev. A, 75 (2007), 063427.
[32] D. Dundas, Phys. Rev. A, 65 (2002), 023408.
[33] K. C. Kulander and F. H. Mies, and K. J. Schafer, Phys. Rev. A, 53 (1996), 2562.
[34] G. L. Ver Steeg and K. Bartschat, and I. Bray, J. Phys. B, 36 (2003), 3325.
[35] I. Kawata, H. Kono, Y. Fujimura, J Chem. Phys., 110 (1999), 11152.
[36] V. Roudnev and B. D. Esry, and I. Ben-Itzhak, Phys. Rev. Lett. , 93 (2004), 163601.
[37] S. Chelkowski, and T. Zuo, and O. Atabek, and A. D. Bandrauk, Phys. Rev. A, 52 (1996), 2977.
[38] K. Liu and W. Hong, and P. Lu, Opt. Express, 19 (2011), 20279.
[39] J. C. Light and T. C. Jr, Adv. Chem. Phys., 114 (2007), 263.
[40] D. J. Tannor, Introduction to quantum mechanics a time-depdentnt perspective, 2000, University Science Books.
[41] T. N. Rescigno and C. W. McCurdy, Phys. Rev. A, 62(2000), 032706.
[42] X. X. Guan, K. Bartschat, and B. I. Schneider, Phys. Rev. A, 83 (2011), 043403.
[43] X. X. Guan, E. B. Secor, K. Bartschat, and B. I. Schneider, Phys. Rev. A, 84 (2011), 033420.
[44] D. Baye and M. Hesse, and M. Vincke, Phys. Rev. E, 65 (2002), 026701.
[45] M. D. Feit and J. A. Fleck, and Jr, J. Comp. Phys.,81 (1983), 3967.
[46] M. M. Madsen and J. M. Peek, Atomic Data , 2 (1971), 171.
[47] D. B. Milošević and G. G. Paulus, and D. Bauer, and W. Becker, J. Phys. B, 39 (2006), R203.

[48] P. F. Lan and P. X. Lu, and F. Li, and Y. H. Li, and Z. Yang, Opt. Express, 16 2008, 5868.
[49] M. Lein, N. Hay, R. Velotta, J. P. Marangos, P. L. Knight, Phys. Rev. A, 66 (2002), 023805.
[50] T. Zuo, A. D. Bandrauk, Phys. Rev. A, 52 (1995), R2511.
[51] M. Vafaee, H. Sabzyan, Z. Vafaee, A. Katanforoush, Phys. Rev. A, 74 (2006), 043416.
[52] I. D. Williams, P. McKenna, B. Srigengan, I. M. Johnston, W. A. Bryant, J. H. Sanderson, A. El-Zein, T. R. J. Goodworth, W. R. Newell, P. F. Taday, A. J. Langley, J. Phys. B, 33 (2000), 2743.
[53] P. Lan, E. J. Takahashi, K. Midorikawa, Phys. Rev. A, 82 (2010) 053413.
[54] P. Colosimo, G. Doumy, C. Blaga, J. Wheeler, C. Hauri, F. Catoire, J. Tate, R. Chirla, A. March, G. G. Paulus, H.G. Muller, P. Agostini, L. F. Dimauro, Nature Phys., 4 (2008), 386.